# Super-atom molecular orbital excited states of fullerenes

PHILOSOPHICAL TRANSACTIONS A

*Phil. Trans. R. Soc. A.***374**: 20150322
doi:10.1098/rsta.2015.0322

# Super-Atom Molecular Orbital Excited States of Fullerenes

**J. Olof Johansson[1], Elvira Bohl[1] and Eleanor E.B. Campbell[1,2]**

*1: EaStCHEM and School of Chemistry, University of Edinburgh, David Brewster Road, Edinburgh EH9 3FJ, U.K.*
*2: Division of Quantum Phases and Devices, School of Physics, Konkuk University, 143-701 Seoul, Korea.*

**Keywords:** Fullerene, SAMO, photoelectron angular distributions

## Summary

Super-atom molecular orbitals (SAMOs) are orbitals that form diffuse hydrogenic excited electronic states of fullerenes with their electron density centred at the centre of the hollow carbon cage and a significant electron density inside the cage. This is a consequence of the high symmetry and hollow structure of the molecules and distinguishes them from typical low-lying molecular Rydberg states. This review summarises the current experimental and theoretical studies related to these exotic excited electronic states with emphasis on femtosecond photoelectron spectroscopy experiments on gas phase fullerenes.
This article is part of the themed issue "Fullerenes: past, present and future, celebrating the 30th anniversary of Buckminsterfullerene".

## 1. Introduction

In the past 30 years since their discovery [1] fullerenes and in particular $C_{60}$ have become very important model systems for studying the properties of complex molecules and nanoparticles in the gas phase. Their ease of handling combined with their high symmetry and chemical simplicity, consisting of only the element carbon, has made them attractive systems for pushing both experimental and theoretical techniques to provide a deeper understanding of the electronic and dynamical properties of matter on the nanoscale. Fullerenes also have the intriguing characteristic that, depending on the experimental circumstances, they can appear to show properties more associated with bulk matter (such as thermionic electron emission) or can appear almost atomic-like [2]. In this review we are focusing on the atomic-like nature of diffuse excited electronic states of fullerenes, known as 'super-atom molecular orbitals" (SAMOs). SAMOs can be considered to be similar to low-lying mixed valence/Rydberg states, often encountered in molecules; however, the hollow and highly symmetric nature of $C_{60}$ provides a spherically symmetric potential with a shallow attractive region in the centre of the molecule. As a consequence of this, the wavefunctions of the lowest members of the lowest angular momenta Rydberg series have significant electron density inside the cage and, in contrast to typical molecular Rydberg states, the electron density is centred on the centre of the hollow cage rather than on the atomic cores that form the molecule. The associated molecular orbitals therefore bare a close resemblance to large, diffuse, nanometer-scale hydrogenic atomic orbitals, Figure 1.

The unusual nature of the SAMOs was first pointed out by Petek and co-workers when they used low-

*Author for correspondence (Eleanor.campbell@ed.ac.uk).

temperature ultrahigh-vacuum scanning tunnel microscopy (STM) to image the orbitals of $C_{60}$ deposited on Cu [3]. The same group also showed the formation of nearly free electron bands when fullerenes aggregated to form a 2D crystal on the metal surface, indicating that these could be interesting systems for molecular electronics applications if the excitation energy of the SAMOs could be tuned to be closer to the Fermi energy. The excited SAMOs were observed earlier in gas-phase $C_{60}$ by femtosecond photoelectron spectroscopy, however, they were not specifically identified as such [4], and they have also been observed in two-photon photoemission (2P-PE) experiments on $C_{60}$ layers deposited on surfaces [5].

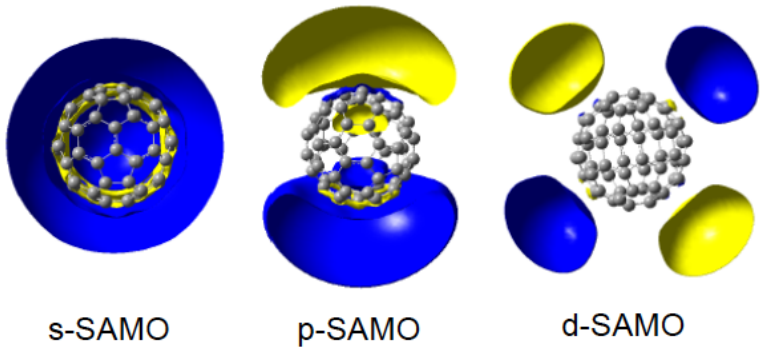


Figure 1. Cuts in the isocontour amplitudes of the Dyson orbitals (representing the probability density of the electron that is ionised) of the s-, p- and d-SAMO states of $C_{60}$. Adapted from [6].

The STM studies have been reviewed previously [7] so here we focus on reviewing the properties of the SAMO states in isolated gas phase molecules where there is no perturbation from the presence of a substrate. We start by briefly reviewing the experimental and theoretical techniques that have been used to obtain information about these excited states in gas-phase molecules before describing the results and finishing with a comparison of experimental photoelectron angular distributions (PADs) with calculations using a simple model potential.

# 2. Methods

The details of the experimental techniques have been provided in previous publications [4, 8, 9] and will be only briefly described here. The original studies that reported the excitation and subsequent single-photon ionisation of Rydberg states in $C_{60}$ were carried out with a combined linear time-of-flight photoelectron spectrometer and a time-of-flight mass spectrometer (MS) [4, 10]. In these earlier studies, the angular dependence of the electron emission was not studied. The emphasis was placed on the determination of the binding energies of the higher-lying members of the Rydberg series that were well resolved using 800nm laser pulses with 1.5 ps duration. In more recent studies, the time-of-flight photoelectron spectrometer was replaced by a velocity map imaging (VMI) spectrometer, illustrated in Fig. 2 [8, 9]. This incorporates a position sensitive detector consisting of a set of multichannel plates followed by a phosphor screen. A CCD camera records the positions at which the electrons arrive on the phosphor screen. The electron extraction voltages are set to produce a 2D projection of the emitted electron cloud on the detector [11]. The resulting images recorded by the CCD camera are inverted to obtain the initial velocity and angular distribution of the electrons using a standard algorithm, either BASEX [12], p-BASEX [13] or Polar-Onion Peeling, POP [14] modified to include up to the tenth Legendre polynomial in the inversion procedure. The great advantage of VMI is that it allows the simultaneous recording of the electron velocity and the PAD. The velocity scale is calibrated by recording the above-threshold ionisation spectrum of Xe. The Xe photoelectron spectra also serve as a convenient calibration for the 800nm laser power [15]. The thermal background was subtracted from the spectra [2] and the SAMO peaks were fitted with Lorentzian functions.

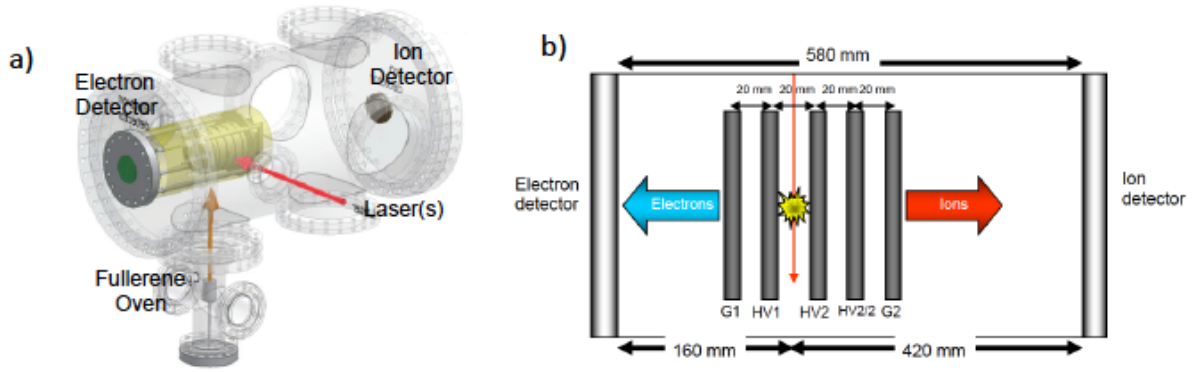


Fig. 2. (a) Schematic diagram of VMI/MS apparatus. (b) Sketch of the electron/ion optics from above.

The laser pulses were obtained from a regenerative amplified Ti:Sapphire laser (*ca*. 110 fs, 800nm). Additional wavelengths were provided by frequency doubling or tripling the fundamental output or by using the fundamental output to pump a commercial non-collinear optical parametric amplifier (NOPA) providing a tunable light source in the visible range. The pulse durations from the NOPA were in the range of 30-90 fs. The laser light was linearly polarised with the electric vector aligned in the vertical direction. In order to obtain a good signal to noise ratio for the SAMO peaks whilst minimising the background contribution due to thermoelectronic ionisation [16], the laser intensity typically was within the range $10^{11} – 10^{12}$ Wcm$^{-2}$.

A number of theoretical approaches for the calculation of the SAMO states have been reported. The early studies focused on characterising the one-electron SAMO orbitals using plane-wave DFT electronic structure calculations [3, 7, 17]. A many-body perturbative approach provided evidence for the enhanced stability and long lifetime of the states [18]. TD-DFT calculations were described in detail by Mignolet *et al*. [19]. In these studies, the electronic structure of the 500 lowest excited states of neutral $C_{60}$ was computed at the TD-DFT/B3LYP/6+31 G(d) [8] or the TD-DFT/CAM-B3LYP/6-31(+)G(d)-Bq(6-31(6+)G(d)) level [19].

Photoelectron spectra, including PADs, were computed by first calculating the Dyson orbitals. The Dyson orbitals are one-particle orbitals computed as the overlap between the neutral and cation many-electron wave functions and represent the probability amplitude of the electron that is ionized [19, 20]. They are used to calculate photoionization intensities and photoelectron angular distributions, as described in detail for $C_{60}$ by Mignolet *et al*. [19]. For $C_{60}$ the SAMO Dyson orbitals, Fig. 1, are very similar to the SAMO molecular orbitals. As the SAMO and Rydberg excited states are composed of several excitations from the highest occupied molecular orbital to several SAMO and/or Rydberg orbitals, the Dyson orbitals of the SAMO and Rydberg states are thus a linear combination of the SAMO/Rydberg molecular orbitals of the same symmetry. The first band of s-SAMO states has a principal quantum number $n = 3$, while the lowest lying members of the p- and d-bands in these calculations, Fig. 1, have $n = 4$ and 5, respectively i.e. all wave functions of the lowest-lying SAMO states contain 2 radial nodes.

# 3. Rydberg fingerprint spectroscopy

The term “Rydberg Fingerprint Spectroscopy” was coined by Weber and co-workers [21]. It refers to the sensitivity of molecular Rydberg electron binding energies to the molecular structure and has been proposed as an analytical technique to distinguish molecular isomers [22] and also as a means of probing isomerisation dynamics on a fs timescale [23]. It was based on the observation that well-

resolved peaks could be observed in the photoelectron spectra of organic molecules corresponding to low-lying molecular Rydberg states when using fs lasers for photoionisation [24, 25]. At the same time, similar observations were made for the excitation and ionisation of Rydberg states of $C_{60}$ [4]. For large molecules like $C_{60}$ where there is a very high density of excited electronic and vibrational states, the excitation is practically independent of the wavelength of the laser used for excitation. An additional advantage of the technique is that, due to the similarity of the Rydberg and cation potential energy surfaces, the final photoionisation step is essentially vibration conserving and the method can work with molecules that have a high initial vibrational energy. A simplified, schematic illustration of the technique is shown in Figure 3. High-lying excited states are very rapidly and efficiently coupled to other excited states, aided by the high degree of vibrational excitation within the molecule and the transient electric field of the laser pulse [26]. This allows the population of a wide band of excited states with varying amounts of vibrational energy, including excited valence states, the fullerene SAMO states and higher lying Rydberg states. Within the same laser pulse, once excited, these SAMO/Rydberg states can be singlephoton ionised by the absorption of an additional photon.

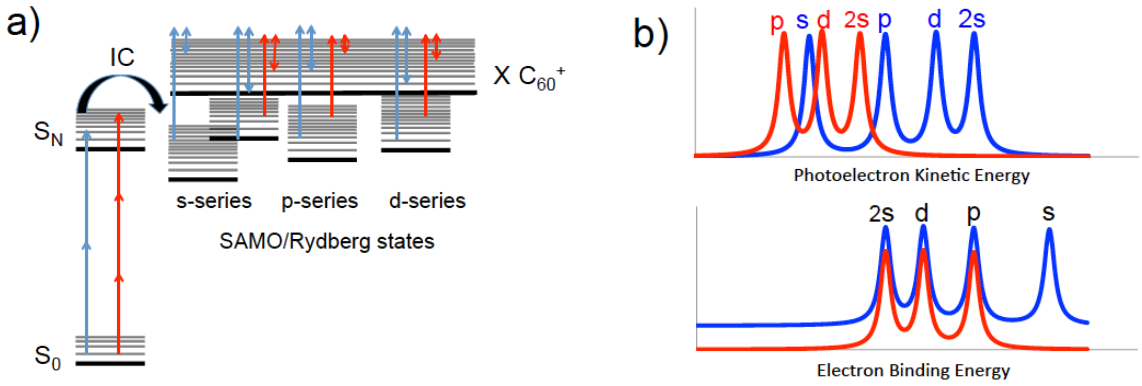


Figure 3. Schematic illustration of the "Rydberg Fingerprint Spectroscopy" technique used to probe the SAMO and Rydberg excited states of the fullerenes. (a) Multiphoton excitation is followed by very efficient state couplings and population of a wide range of excited states with varying amounts of vibrational energy. Narrow lines indicate vibrational excitation. Only the first two members of the s-series and the first members of the p- and d-series are shown for clarity. The single headed arrows indicate two different photon energies. The double-headed arrows indicate the photoelectron kinetic energies. Note that the photon energy corresponding to the red arrow is too low to ionise the lowest-lying s-state. (b) Upper: schematic illustration of the photoelectron spectra that would be observed for the two photon energies shown in (a). Lower: corresponding electron binding energies.

Since the excited states are incoherently populated, the final step in the photoionisation process can be considered to be a single-photon ionisation from the excited states. In this case the photoelectron angular distribution for a random orientation of the molecule can be described as [27]

$$I(\theta) \propto \left(1 + \beta \, \mathrm{P}_2(\cos\theta)\right) \qquad (1)$$

where $\beta$ is an anisotropy parameter, taking values within the range -1 to +2, and $P_2(\cos\theta)$ is the second order Legendre polynomial.

# 4. Fullerene super-atom molecular orbitals and Rydberg States

Owing to the unique hollow nature of the fullerenes, the low-lying members of Rydberg series, the

SAMOs, which are the main interest here, are rather unusual in having the electron density centred on the centre of the hollow molecular core rather than on the atomic constituents of the molecule. SAMOs arise because of the hollow core potential defined by the spherical $C_{60}$ carbon cage. The overall potential is a sum of two contributions: the deep Coulomb wells centered on each carbon atom and a shallow attractive potential induced by the long-range-dispersion interactions between electrons localized on two opposite sides of the cage. While only the former is sufficient to define the σ and π molecular orbitals, the shallow attractive potential within the cage is essential for correctly describing SAMO states. In particular, the lowest-lying members of the s- and p-series are considered to have significant electron density within the centre of the molecule (see Fig. 1). The s-SAMO has even been identified theoretically for anions [28, 29]. This clearly distinguishes the SAMO states from the higher-lying Rydberg states. The unique nature of the potential was discussed in analogy with image potential states of graphene in the context of the STM experiments carried out by the Petek group [7]. For states with higher principal quantum numbers the electron density is almost entirely outside the carbon cage and the electron binding energies and properties more closely resemble that of conventional Rydberg series.

A series of VMI images and the corresponding angle-integrated photoelectron spectra, plotted as a function of electron binding energy ($E_{bind} = h\nu - E_{kin}$, where $h\nu$ is the photon energy) rather than photoelectron kinetic energy ($E_{kin}$) , are shown in Figure 4 for $C_{60}$ for three different laser wavelengths. The peak structure is clearly seen in all three spectra with the most prominent peak (assigned to the excitation of the first s-SAMO band) being indicated by the dashed red lines. The positions of the maxima of the first p- and d- bands and the second s-band are indicated by the vertical dashed lines. This series of measurements nicely illustrates the non-resonant nature of the excitation of the SAMO states as well as the single-photon ionisation from the excited states that underpins the analysis and interpretation.

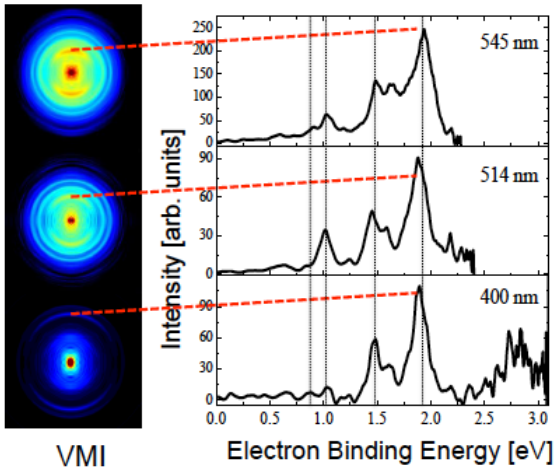


Figure 4. VMI images and the corresponding angle-integrated photoelectron spectra for $C_{60}$, plotted as a function of electron binding energy, for ionisation with three different laser wavelengths: 545 nm, 514nm and 400nm (top to bottom).

The experimentally measured electron binding energies are given in Table 1 along with calculated values. The plane-wave DFT values [3] were only given with respect to the calculated lowest unoccupied molecular orbital value and are, therefore, just given as energy differences between the states. The experimental assignment was based partly on the calculated binding energies and partly on the photoelectron angular distributions. The experimental angular distributions were extracted by dividing the VMI data into angular segments and integrating the relevant peak intensity in each case [9]. An example for the peak at a binding energy of 1.9 eV, indicated in Fig. 4, is shown in Figure 5(a) for the 400nm data with the data fitted to equation (1).

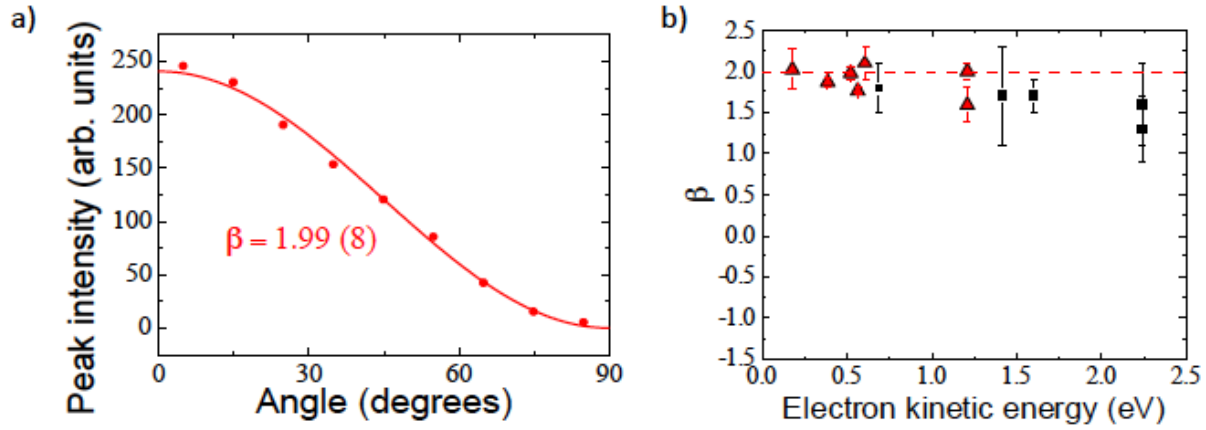


Figure 5. (a) Photoelectron angular distribution for the peak in the 400nm photoelectron spectrum shown in Fig. 4 at a binding energy of 1.9 eV. (b) Value of the anisotropy parameter, $\beta$, as a function of photoelectron kinetic energy for the peaks assigned to the first (red, triangles) and second (black, squares) members of the s-SAMO series. The data point corresponding to the plot in (a) appears at an electron kinetic energy of $E_{kin} = h\nu - E_{bind} = 3.1 - 1.9 = 1.2$ eV.

The value extracted for the anisotropy parameter, $\beta$, for the peaks with binding energies of 1.9 $\pm$0.1 eV shows that the outgoing electron is very close to a pure p-wave. This is expected for single-photon ionisation from an s-state with zero orbital angular momentum ($\ell = 0$). An additional confirmation of the assignment of this peak is obtained when considering the extracted value of $\beta$ as a function of the kinetic energy of the outgoing electron. For ionisation from an s-state, the value of $\beta$ should not change as the electron kinetic energy changes since the outgoing wave should always be a p-wave. The non-resonant excitation mechanism for the SAMOs allows us to test this by simply changing the wavelength of the laser. The results are shown in Fig. 5(b) for the peaks assigned to the first (binding energy 1.9 eV) and second (binding energy 0.87 eV) members of the s-series. The situation is less straightforward for ionisation from states with higher values of the orbital angular momentum since more than one exit channel is possible ($\Delta\ell = \pm 1$) and the value will change as the velocity of the outgoing electron changes. In this situation, comparison with the theoretical results helps to assign the peaks.

A comparison of the experimentally determined anisotropy parameters and TD-DFT calculations for the B3LYP/6+31 G(d) and CAM-B3LYP/6-31(+)G(d)-Bq(6-31(6+)G(d)) level is shown in Figure 6 for $C_{60}$, and $C_{70}$ with additional experimental values for $C_{82}$ and $Sc_3N@C_{80}$.

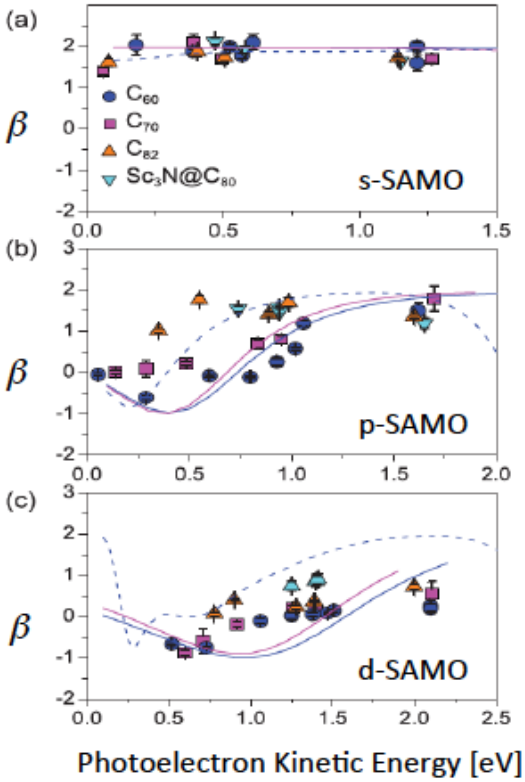


Figure 6. Photoelectron angular distributions (PADs) for (a) s-states, (b) p-states, and (c) d-states, characterised by the fitted $\beta$ value for experiments on $C_{60}$ (circles), $C_{70}$ (squares), $C_{82}$ (up-triangles), $Sc_3N@C_{80}$ (down-triangles). The full lines show the calculated $\beta$-values for $C_{60}$ and $C_{70}$ at the B3LYP/6-31+G(d) level [8]. The dashed lines are $C_{60}$ CAM-B3LYP/6-31(+)G(d)-Bq(6-31(6+)G(d)) results [19]. Adapted from [9].

Both the experimental and theoretical results are almost identical for $C_{60}$ and $C_{70}$. Although the CAM-B3LYP/6-31(+)G(d)-Bq(6-31(6+)G(d)) calculations provide better agreement with the experimental binding energies, the B3LYP/6-31+G(d) angular distributions are in better agreement with the measurements for the p-SAMO. The d-SAMO measurements lie in between the two sets of calculations. The predicted angular distributions are very sensitive to the diffusivity of the wavefunctions. The angular distributions for ionisation from the p-SAMO are significantly shifted for low kinetic energies for $C_{82}$ and $Sc_3N@C_{80}$ with respect to $C_{60}$ and $C_{70}$. A smaller, but still significant, shift is also seen for the d-SAMO.

Photoelectron spectra parallel and perpendicular to the laser polarisation direction are compared for the different fullerenes whose $\beta$-values are plotted in Fig. 6, obtained at a wavelength of around 500nm, in Figure 7. The binding energies of the SAMO peaks are very similar in all cases (Table 1). It should be noted that the ionisation energies of the higher fullerenes and the endohedral species are all significantly lower than that of $C_{60}$; therefore, the excitation energy of the SAMO states must be lowered by the same amount. The main difference in the photoelectron spectra is a broadening of the peak widths and a more prominent double-peak structure for the p-SAMO band due to the decreasing symmetry as the size of the fullerene cage is increased. The peak structure for the first s- and p-SAMO bands is almost completely smeared out for the endohedral fullerene, $Sc_3N@C_{80}$ [9].

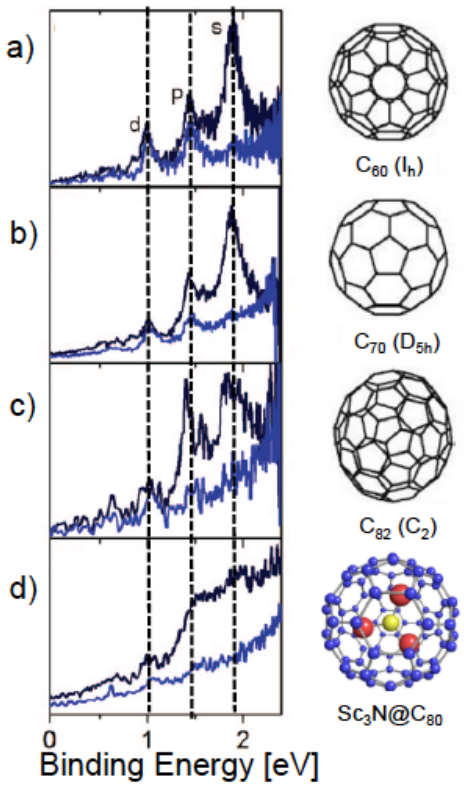


Figure 7. Photoelectron spectra parallel (black) and perpendicular (blue) to the laser polarisation direction of (a) $C_{60}$, 500 nm, 4.7 $TWcm^{-2}$ (b) $C_{70}$, 520 nm 2.9 $TWcm^{-2}$ (c) $C_{82}$, 519nm, 2.8 $TWcm^{-2}$ (d) $Sc_3N@C_{80}$, 506nm 4.1 $TWcm^{-2}$. Adapted from [9].

The TD-DFT calculations also provided insight into the dominance of peaks corresponding to single-photon ionisation of SAMO bands over valence bands in the photoelectron spectra. The photoionisation widths between the excited electronic states and the ground state of the cation were computed using a basis of orthogonalised plane waves to describe the wave function of the ionised electron [19]. The photoionisation width was computed for each state taking into account the random orientation of the $C_{60}$ molecule with respect to the electric field. The calculated photoionisation width is proportional to the photoionisation rate and directly related to the photoionisation cross-section (it does not refer to the width of the peaks in the photoelectron spectrum).

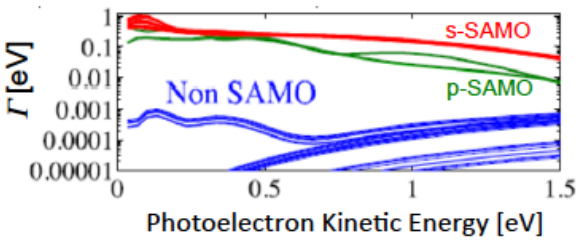


Figure 8. Photoionisation widths, $\Gamma$, plotted on a logarithmic scale versus the photoelectron kinetic energy. Adapted from [19].

For the relatively low photoelectron kinetic energies that are studied in these experiments, the photoionisation cross section from the SAMO states is orders of magnitude larger than ionisation from the non-SAMO valence excited states. The calculated photoionisation widths can be converted to photoionisation lifetimes on the order of femtoseconds for the SAMO states but picoseconds to nanoseconds for the non-SAMO states [19]. This explains very clearly why the SAMO peaks are so

dominant for ionisation with visible laser wavelengths. Even though the non-SAMO states will be populated, the probability that they will be single-photon ionised on the timescale of the laser pulse (50-100 fs) is vanishingly small.

The ratio of calculated photoionisation widths has been compared to relative experimental ionisation intensities [6]. The results, Figure 9, show very good agreement between the theoretical ratios and the experimental ratios for photon energies where the same number of photons can access both states. Outside these regions, the s-band can be accessed by one less photon than the higher states. In this case the s-band intensity would be expected to be significantly higher than the higher-lying states and the measured ratios are correspondingly higher. This is not accounted for by the calculations because they do not include the population mechanism but simply assume that all states are populated with the same probability. The results are quite remarkable because they are implying that this assumption (at least for the SAMO population) does hold as long as the photon order needed to energetically access the states is the same. What is apparent is that the TD-DFT calculations are, with good accuracy, able to predict the photoionisation probability in addition to the PAD as a function of kinetic energy as discussed earlier.

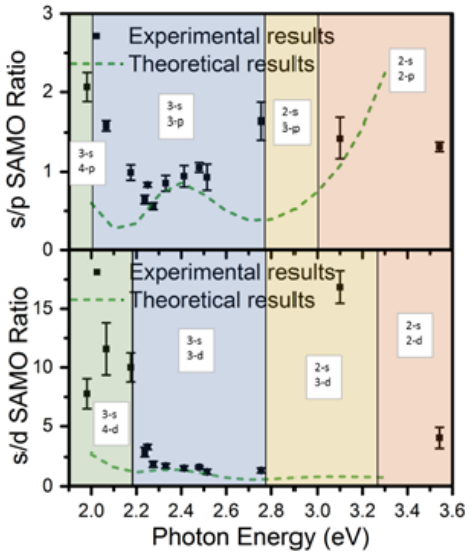


Figure 9. Comparison of relative experimental SAMO peak intensities (squares) and the theoretical photoionisation width ratios of SAMO states plotted as a function of laser photon energy. Upper panel: ratio of the s and p peak intensities. Lower panel: ratio of the s and d peak intensities. Theoretical values shown by dashed lines (ratio of average values calculated for each band). The numbers in each panel indicate the number of photons needed to access the s and the p or d SAMO states, respectively. Adapted from [6].

The rapid decrease in the photoionisation width of the SAMO/Rydberg states as the photoelectron kinetic energy increases (Fig. 8) also explains why the higher lying Rydberg states that were the subject of the early studies [4, 10, 30] are much less prominent for excitation with visible light. Excitation and ionisation with 800nm 1.5 ps bandwidth limited picosecond laser pulses produced photoelectron spectra where the higher lying states were well resolved [4]. The assignment of the peaks was made by comparing the experimental binding energies with the numerical solution of the Schrödinger equation using a simple model potential [4]. In light of the detail that can be obtained in angle-resolved studies using VMI it would be useful to revisit the study of the higher lying Rydberg states using picosecond ionisation.

# 5. Photoelectron angular distributions from a phenomenological potential

There have been a number of attempts to model $C_{60}$ and $X@C_{60}$ photoionisation using simple, spherically symmetric, phenomenological potentials [4, 7, 31-33]. Usually in these studies, the depth, width and shape of the potential well is adjusted to fit the experimental results and has often taken the form of a quasi-square well potential at the position of the carbon atoms. For example, the model used to calculate the Rydberg binding energies, discussed above was based on a quasi-rectangular potential at the position of the carbon atoms, published by Puska and Nieminen [34]. In order to illustrate the use of a phenomenological potential to model the PADs, we have adapted a phenomenological square well potential to have a shallow attractive core and adjusted the parameters to obtain good agreement with the SAMO binding energies. We then numerically solve the Schrödinger potential within Matlab, following the method described by Falkensteiner et al. [35]. The eigenenergies for the lowest s, p and d SAMO states are given in Table 1. The corresponding wave functions were then used to calculate the photoelectron angular distributions following the method described by Bartels et al. [36].

The anisotropy parameter, $\beta$, is defined within the Bethe-Cooper-Zare theory [37, 38] as

$$\beta = \frac{\ell(\ell-1)R_-^2+(\ell+1)(\ell+2)R_+^2-6\ell(\ell+1)R_-R_+cos\delta}{(2\ell+1)\left(\ell R_-^2+(\ell-1)R_+^2\right)} \quad (2)$$

where

$$R_\pm = \int \psi_f^\pm(r)\psi_i(r)r^3dr \quad (3)$$

are the radial matrix elements, $\psi_i$ and $\psi_f$ are the initial and final state wave functions, $\ell$ is the orbital angular momentum quantum number of the initial state, $r$ is the radial coordinate, and $\delta = \delta_+ - \delta_-$ is the difference of the Coulomb phase shifts of the final state wave functions $\psi_f$, defined by their asymptotic behavior [39]. The $\pm$ subscripts refer to the $\ell$+1 and $\ell$ -1 transitions.

$$R_\pm \simeq \sqrt{\frac{2}{\pi k}}\frac{1}{r}cos\left(kr-(\ell\pm1)\frac{\pi}{2}+\frac{\log(2kr)}{k}+\delta_\pm+\sigma_\pm\right) \text{ for } r\longrightarrow\infty\,. \quad (4)$$

Here, $k$ is the magnitude of the wavevector and $\sigma$ is the Coulomb phase ($= \arg\Gamma(1+\ell-i/k)$) [40].

The results for the lowest s, p and d SAMOs are shown in Figure 10. The spherically symmetric radial potential used for the calculations is shown as an inset in the lower plot. The results are rather close to the experimental values. It should be noted that although quasi-square well potentials have been used to model fullerene photoionisation they are not very physical and a cusp-like potential has been suggested as a more realistic approximation [41]. The good agreement achieved here gives some confidence that a systematic comparison of the eigenenergies and angular distributions obtained from the available model potentials should provide a means of selecting the most appropriate and generally applicable model potential for $C_{60}$.

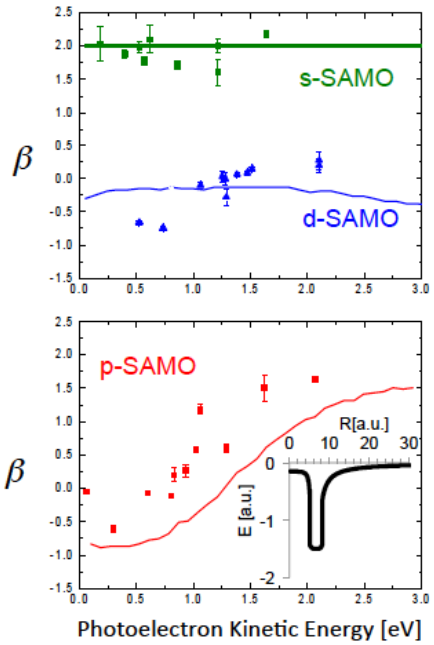


Figure 10. Comparison of experimental anisotropy parameters, $\beta$, with calculations using the simple phenomenological model potential shown in the inset. Note that the beta value for the s-SAMO is independent of the potential, which can be seen from Eq. (2).

# 6. Conclusion

Thirty years after their discovery, fullerenes continue to be valuable model systems and serve to develop new experimental and theoretical techniques that can probe ever more complex systems. The fullerene SAMO excited electronic states that have been reviewed here provide large, challenging systems for quantum chemistry but, most attractively, the high symmetry and nature of the $C_{60}$ molecules also makes it possible to apply much simpler models that provide more intuitive insight into the factors that influence the binding energy of these interesting states. The increased knowledge of the properties of these states may lead to design of materials for specific charge transport applications and may also play an important role in understanding the chemistry of neutral and charged fullerenes in space.

# Additional Information

**Acknowledgments**

We thank Françoise Remacle and Benoit Mignolet (University of Liège) for supplying the TD-DFT calculations and for many fruitful discussions. We also thank James Thompson, Gordon Henderson and Katarzyna Sokół for their contributions to the experiments.

**Funding Statement**

Funding from the Leverhulme Trust (RPF-298 "PES of hollow nanomaterials") is gratefully acknowledged. EEBC acknowledges the support of a JILA Visiting Fellowship. JOJ is a Royal Society of Edinburgh/BP Trust research fellow.

**Competing Interests**

We have no competing interests.

**Authors' Contributions**

JOJ and EB carried out the experimental work, analysed the experimental data and contributed to data interpretation. JOJ solved the Schrödinger equation for the simple jellium model and calculated the corresponding photoelectron angular distributions EEBC designed the experiments, supervised the research, contributed to data interpretation and wrote the manuscript.

# References


1. Kroto HW, Heath JR, O'Brien SC, Curl RF, Smalley RE. 1985; $C_{60}$: Buckminsterfullerene. Nature. **318**: 162-3.
2. Johansson JO, Campbell EEB. 2013; Probing excited electronic states and ionisation mechanisms of fullerenes. Chemical Society Reviews. **42**: 5661-71. (10.1039/C3CS60047E)
3. Feng M, Zhao J, Petek H. 2008; Atom like, Hollow-Core-Bound Molecular Orbitals of $C_{60}$. Science. **320**: 359-62.
4. Boyle M, Hoffmann K, Schulz CP, Hertel IV, Levine RD, Campbell EEB. 2001; Excitation of Rydberg Series in $C_{60}$. Phys Rev Lett. **87**: 273401.
5. Dutton GJ, Dougherty DB, Jin W, Reutt-Robey JE, Robey SW. 2011; Superatom orbitals of $C_{60}$ on Ag(111): Two-photon photoemission and scanning tunneling spectroscopy. Phys Rev B. **84**: 195435.
6. Bohl E, Sokół KP, Mignolet B, Thompson JOF, Johansson JO, Remacle F, et al. 2015; Relative Photoionization Cross Sections of Super-Atom Molecular Orbitals (SAMOs) in $C_{60}$. J Phys Chem A. **119**: 11504-8. (10.1021/acs.jpca.5b10339)
7. Feng M, Zhao J, Huang T, Zhu X, Petek H. 2011; The electronic properties of superatom states of hollow molecules. Acc Chem Res. **44**: 360-8. (10.1021/ar1001445)
8. Johansson JO, Henderson G, Remacle F, Campbell EEB. 2012; Angular-resolved Photoelectron Spectroscopy of Superatom Orbitals of Fullerenes. Phys Rev Lett. **108**: 173491. (10.1103/PhysRevLett.108.173401)
9. Johansson JO, Bohl E, Henderson GG, Mignolet B, Dennis TJS, Remacle F, et al. 2013; Hot electron production and diffuse excited states in $C_{70}$, $C_{82}$, and $Sc_3N@C_{80}$ characterized by angular-resolved photoelectron spectroscopy. J Chem Phys. **139**: 084309. (doi:http://dx.doi.org/10.1063/1.4818987)
10. Boyle M, Laarmann T, Hoffmann K, Hedén M, Campbell EEB, Schulz CP, et al. 2005; Excitation dynamics of Rydberg states in $C_{60}$. Eur Phys J D. **36**: 339-51.
11. Bordas C, Paulig F, Helm H, Huestis DL. 1996; Photoelectron imaging spectrometry: Principle and inversion method. Rev Sci Instr. **67**: 2257-68.
12. Dribinski V, Ossadtchi A, Mandelshtam VA, Reisler H. 2002; Reconstruction of Abel-transformable images: The Gaussian basis-set expansion Abel transform method. Rev Sci Instr. **73**: 2634-42. (doi:http://dx.doi.org/10.1063/1.1482156)
13. Garcia GA, Nahon L, Powis I. 2004; Two-dimensional charged particle image inversion using a polar basis function expansion. Rev Sci Instr. **75**: 4989-96. (doi:http://dx.doi.org/10.1063/1.1807578)
14. Roberts GM, Nixon JL, Lecointre J, Wrede E, Verlet JRR. 2009; Toward real-time charged-particle image reconstruction using polar onion-peeling. Rev Sci Instr. **80**: 053104. (doi:http://dx.doi.org/10.1063/1.3126527)
15. Schyja V, Lang T, Helm H. 1998; Channel switching in above-threshold ionization of xenon. Phys Rev A. **57**: 3692-7.
16. Johansson JO, Fedor J, Goto M, Kjellberg M, Stenfalk J, Henderson GG, et al. 2012; Anisotropic hot electron emission from fullerenes. J Chem Phys. **136**: 164301. (10.1063/1.4704828)
17. Zhao J, Feng M, Yang J, Petek H. 2009; The Superatom States of Fullerenes and Their Hybridization into the Nearly Free Electron Bands of Fullerites. ACS Nano. **3**: 853-64.
18. Pavlyukh Y, Berakdar J. 2011; Communication: Superatom molecular orbitals: New types of long-lived electronic states. J Chem Phys. **135**: 201103. (doi:http://dx.doi.org/10.1063/1.3665089)
19. Mignolet B, Johansson JO, Campbell EEB, Remacle F. 2013; Probing Rapidly-Ionizing Super-Atom Molecular Orbtals in $C_{60}$: A Computational and Femtosecond Photoelectron Spectroscopy Study. ChemPhysChem. **14**: 3332-40. (10.1002/cphc.201300585)

20. Dauth M, Wiessner M, Feyer V, Schöll A, Puschnig P, Reinert F, et al. 2014; Angle resolved photoemission from organic semiconductors: orbital imaging beyond the molecular orbital interpretation. New Journal of Physics. **16**: 103005.
21. Gosselin JL, Weber PM. 2005; Rydberg Fingerprint Spectroscopy: A New Spectroscopic Tool with Local and Global Structural Sensitivity. J Phys Chem A. **109**: 4899-904. (10.1021/jp0503866)
22. Cardoza JD, Rudakov FM, Hansen N, Weber PM. 2008; Identification of isomeric hydrocarbons by Rydberg photoelectron spectroscopy. J Electron Spectr Rel Phen. **165**: 5-10. (http://dx.doi.org/10.1016/j.elspec.2008.06.003)
23. Rudakov FM, Weber PM. 2012; Ultrafast structural and isomerization dynamics in the Rydberg-exited Quadricyclane: Norbornadiene system. J Chem Phys. **136**: 134303. (doi:http://dx.doi.org/10.1063/1.3697472)
24. Schick CP, Weber PM. 2001; Ultrafast Dynamics in the Three-Photon, Double-Resonance Ionization of Phenol via the $S_2$ Electronic State. J Phys Chem A. **105**: 3735-40. (10.1021/jp003304g)
25. Tsubouchi M, Whitaker BJ, Wang L, Kohguchi H, Suzuki T. 2001; Photoelectron Imaging on Time-Dependent Molecular Alignment Created by a Femtosecond Laser Pulse. Phys Rev Lett. **86**: 4500-3.
26. Zhang GP, Sun X, George TF. 2003; Laser-induced ultrafast dynamics in $C_{60}$. Phys Rev B. **68**: 165410.
27. Cooper J, Zare RN. 1968; Angular distribution of photoelectrons. J Chem Phys. **48**: 942-3.
28. Klaiman S, Gromov EV, Cederbaum LS. 2013; Extreme Correlation Effects in the Elusive Bound Spectrum of $C_{60}^-$. J Phys Chem Lett. **4**: 3319-24. (10.1021/jz4018514)
29. Voora VK, Cederbaum LS, Jordan KD. 2013; Existence of a Correlation Bound s-Type Anion State of $C_{60}$. J Phys Chem Lett. **4**: 849-53. (10.1021/jz400195s)
30. Boyle M, Hedén M, Schulz CP, Campbell EEB, Hertel IV. 2004; Two-color pump-probe study and internal-energy dependence of Rydberg-state excitation in $C_{60}$. Phys Rev A. **70**: 051201.
31. Dolmatov VK, Baltenkov AS, Connerade JP, Manson ST. 2004; Structure and photoionization of confined atoms. Rad Phys Chem. **70**: 417-33. (http://dx.doi.org/10.1016/j.radphyschem.2003.12.024)
32. Madjet ME, ChakrabortY HS, Rost JM, Manson ST. 2008; Photoionization of $C_{60}$: a model study. J PhysB: Atomic, Molecular and Optical Physics. **41**: 105101.
33. Phaneuf RA, Kilcoyne ALD, Aryal NB, Baral KK, Esteves-Macaluso DA, Thomas CM, et al. 2013; Probing confinement resonances by photoionizing Xe inside a $C_{60}$ molecular cage. Phys Rev A. **88**: 053402.
34. Puska MJ, Nieminen RM. 1993; Photoabsorption of atoms inside $C_{60}$. Phys Rev A. **47**: 1181-6.
35. Falkensteiner P, Grosse H, Schöberl F, Hertel P. 1985; Solving the Schrödinger equation for bound states. Computer Physics Communications. **34**: 287-93. (http://dx.doi.org/10.1016/0010-4655(85)90005-0)
36. Bartels C, Hock C, Huwer J, Kuhnen R, Schwöbel J, von Issendorff B. 2009; Probing the Angular Momentum Character of the Valence Orbitals of Free Sodium Nanoclusters. Science. **323**: 1323-7.
37. Cooper J, Zare RN. 1968; Angular Distribution of Photoelectrons. J Chem Phys. **48**: 942-3. (doi:http://dx.doi.org/10.1063/1.1668742)
38. Cooper J, Zare RN. 1968; Erratum: Angular Distribution of Photoelectrons. J Chem Phys. **49**: 4252-. (doi:http://dx.doi.org/10.1063/1.1670761)
39. Bethe HA, Salpeter EE. Quantum Mechanics of One- and Two-Electron Atoms. New York: Plenum Publishing Corporation; 1977.
40. Hertel IV, Schulz CP. Atoms, Molecules and Optical Physics 1. Berlin Heidelberg: Springer Verlag; 2015.
41. Baltenkov AS, Manson ST, Msezane AZ. 2015; Jellium model potentials for the $C_{60}$ molecule and the photoionization of endohedral atoms, A@$C_{60}$. J Phys B: Atomic, Molecular and Optical Physics. **48**: 185103.

# Table 1. Comparison of Experimental and Theoretical Binding Energies for the $C_{60}$ SAMOs

| | SAMO Binding Energy /eV | | | | | | |
|---|---|---|---|---|---|---|---|
| | s | $\Delta_{sp}$ | p | $\Delta_{pd}$ | d | $\Delta_{ds'}$ | s' |
| Experiment [8] | 1.90± 0.01 | 0.43 | 1.47± 0.02 | 0.45 | 1.02± 0.01 | 0.15 | 0.87± 0.02 |
| B3LYP 6-31+G(d) [8] | 2.15 | 0.89 | 1.26 | 0.49 | 0.77 | -0.01 | 0.78 |
| CAM-B3LYP 6-31+G(D)+diff. [19] | 2.35 | 0.89 – 0.63 | 1.46-1.72 | 0.11 – 0.58 | 1.14-1.35 | 0 | 1.14-1.35 |
| Plane-wave DFT | | 0.66 | | 0.55 | | -0.1 | |
| Model potential | 1.9 | 0.3 | 1.6 | 0.6 | 1.0 | 0.1 | 0.9 |